Appendix

In situ and high-resolution Cryo-EM structure of the Type VI secretion membrane complex

Chiara Rapisarda[1,2]*, Yassine Cherrak [3]*, Romain Kooger[4]*, Victoria Schmidt[3], Riccardo Pellarin[5], Laureen Logger[3], Eric Cascales[6], Martin Pilhofer[4#], Eric Durand[3#], Rémi Fronzes[1,2#]

[1]CNRS UMR 5234 Microbiologie Fondamentale et Pathogénicité, Paris, France.
[2]Institut Européen de Chimie et Biologie, University of Bordeaux, 2 rue Robert Escarpit, 33607, Pessac, France.
[3]Laboratoire d'Ingénierie des Systèmes Macromoléculaires (LISM), Institut de Microbiologie de la Méditerranée (IMM), UMR7255, Aix-Marseille Université - CNRS, Marseille, France.
[4]Institute of Molecular Biology & Biophysics, Eidgenössische Technische Hochschule Zürich, CH-8093 Zürich, Switzerland
[5]Institut Pasteur, Structural Bioinformatics Unit, Department of Structural Biology and Chemistry, CNRS UMR 3528, C3BI USR 3756, Paris, France.
[6]Laboratoire d'Ingénierie des Systèmes Macromoléculaires (LISM), Institut de Microbiologie de la Méditerranée (IMM), UMR7255, INSERM - Marseille, France.

*these authors contributed equally to the work
[#] corresponding authors: pilhofer@biol.ethz.ch, edurand@imm.cnrs.fr & edurand@inserm.fr and r.fronzes@iecb.u-bordeaux.fr

Table of contents:

Supplementary figures

Appendix Figure S1

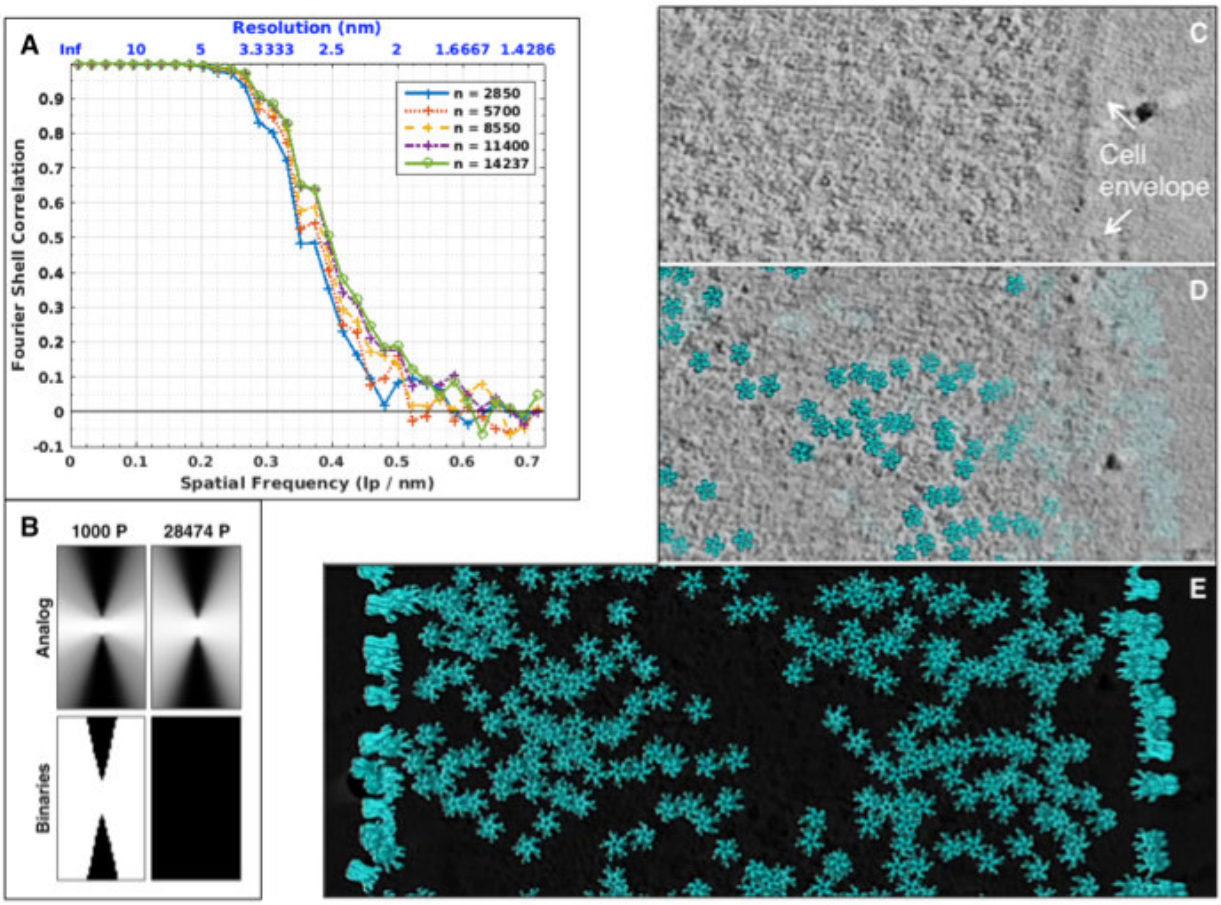

Sub-tomogram average validation and the TssJLM average placed back into a tomogram.

A FSC curve of the C5-symmetrized final average generated in the PEET software package. The *n* value in the top right box corresponds to the number of particles in each of the two equal-sized groups whose averages are being compared in the Fourier space

B Wedge weight generated in the PEET software package. The binaries had the threshold set to simply show which planes in Fourier space were considered present and which were not, while the analog version shows intensities proportional to the number of samples. The dark rectangle bottom right shows that all planes were considered present in the Fourier space, but the analog representation shows an over-representation of some planes. This indicates a missing wedge in our average that could be reflected in the elongation of the neck region of the average (Appendix Fig S9A right, light pink) compared to the SPA structure (Appendix Fig S9B left, carmine)

C-E Slice (17.1 nm) through the tomogram of a single *E. coli* BL21 ghost cell in which TssJLM was overexpressed heterogously. The average was placed back in the tomogram at the individual positions and orientations that were used to generate the final average (turquoise, same isosurface as in Fig 1). (C) shows the tomogram on its own, (E) shows only the isosurfaces and (D) shows the isosurface merged in the tomogram. Top, bottom and side views could be seen. The cell envelope is indicated by white arrows. Scale bar 100 nm

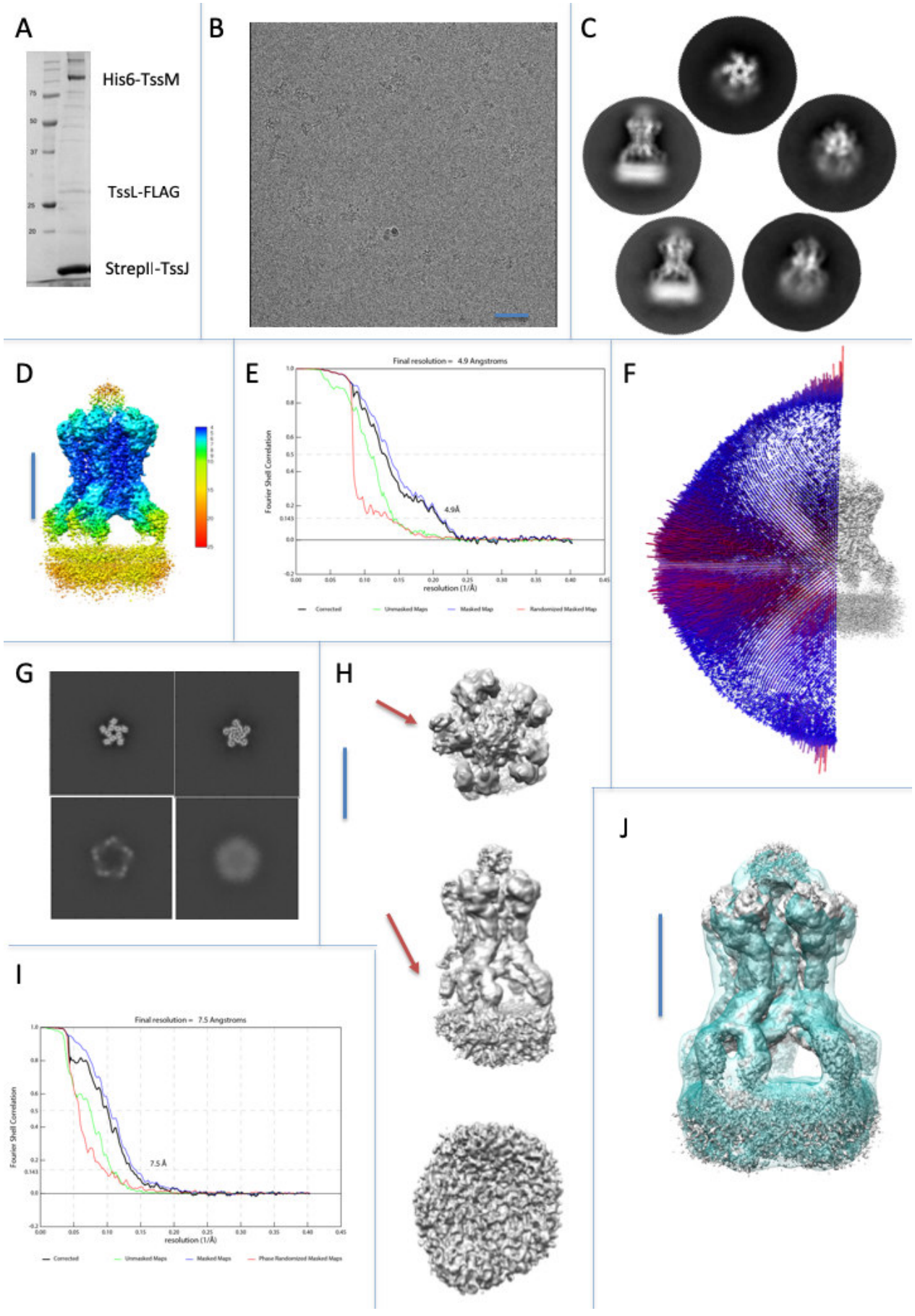
A
His6-TssM
TssL-FLAG
StrepII-TssJ
B
C
D
E
Final resolution = 4.9 Angstroms
Fourier Shell Correlation
4.9Å
resolution (1/Å)
Corrected
Unmasked Maps
Masked Map
Randomized Masked Map
F
G
H
I
Final resolution = 7.5 Angstroms
Fourier Shell Correlation
7.5 Å
resolution (1/Å)
Corrected
Unmasked Maps
Masked Maps
Phase Randomized Masked Maps
J

Appendix Figure S2

Single particle cryo-EM of the membrane complex

A Coomassie stained 12% SDS gel of the TssJLM after purification.

B Representative micrograph of the TssJLM complex in ice, as imaged on the Talos Arctica. The scale bar represents 50 nm

C 2D classes of the TssJLM complex in ice, aligned according to their orientation

D 3D cryo-EM density autosharpened with Phenix, and coloured according to local resolution. The scale bar represents 100 Å

E FSC curve of the full complex reconstruction with a C5 symmetry imposed, as calculated with postprocess in Relion 2

F Angular distribution of the cryo-EM reconstruction

G Slices through the 3D cryo-EM density

H Cryo-EM density of the full complex with no symmetry applied. Three orientations are shown. Red arrows point to the missing density. The scale bar represents 100 Å

I FSC curve of the full complex reconstruction in C1, as calculated with postprocess in Relion 2

J Superimposition of the negative stain 3D reconstruction in cyan (EMD-2927) and the high-resolution, unsharpened cryo-EM reconstruction with C5 symmetry imposed

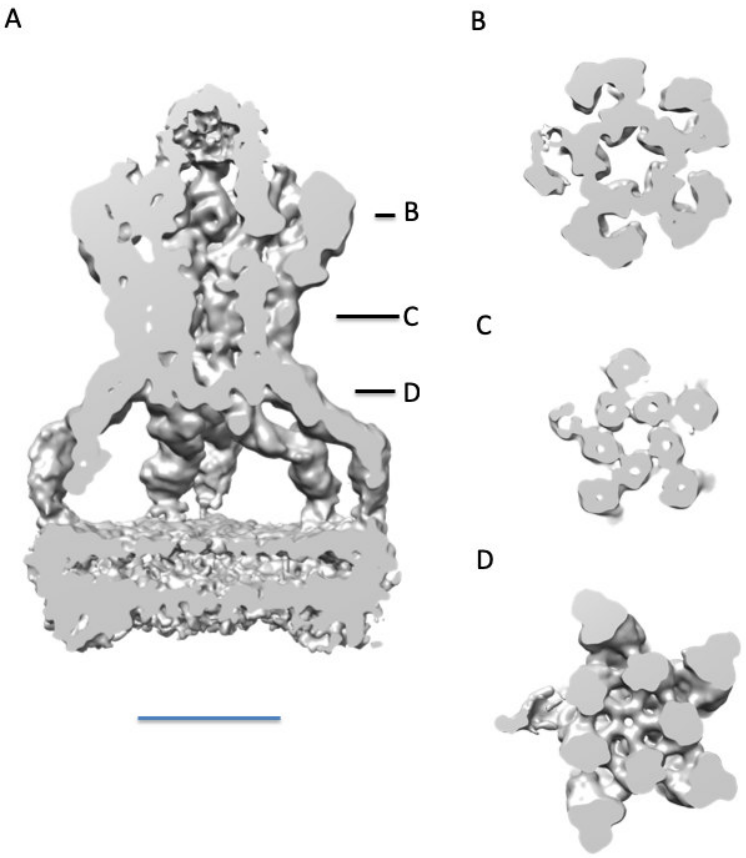

Appendix Figure S3

Analysis of the cryo-EM density in C1 symmetry

A Cross-section of the cryo-EM density reconstructed using a C1 symmetry. Positions of slices B-D are indicated with black lines. The scale bar represents 100 Å

B-D Cross-sections of A, at positions indicated by black lines and labelled accordingly

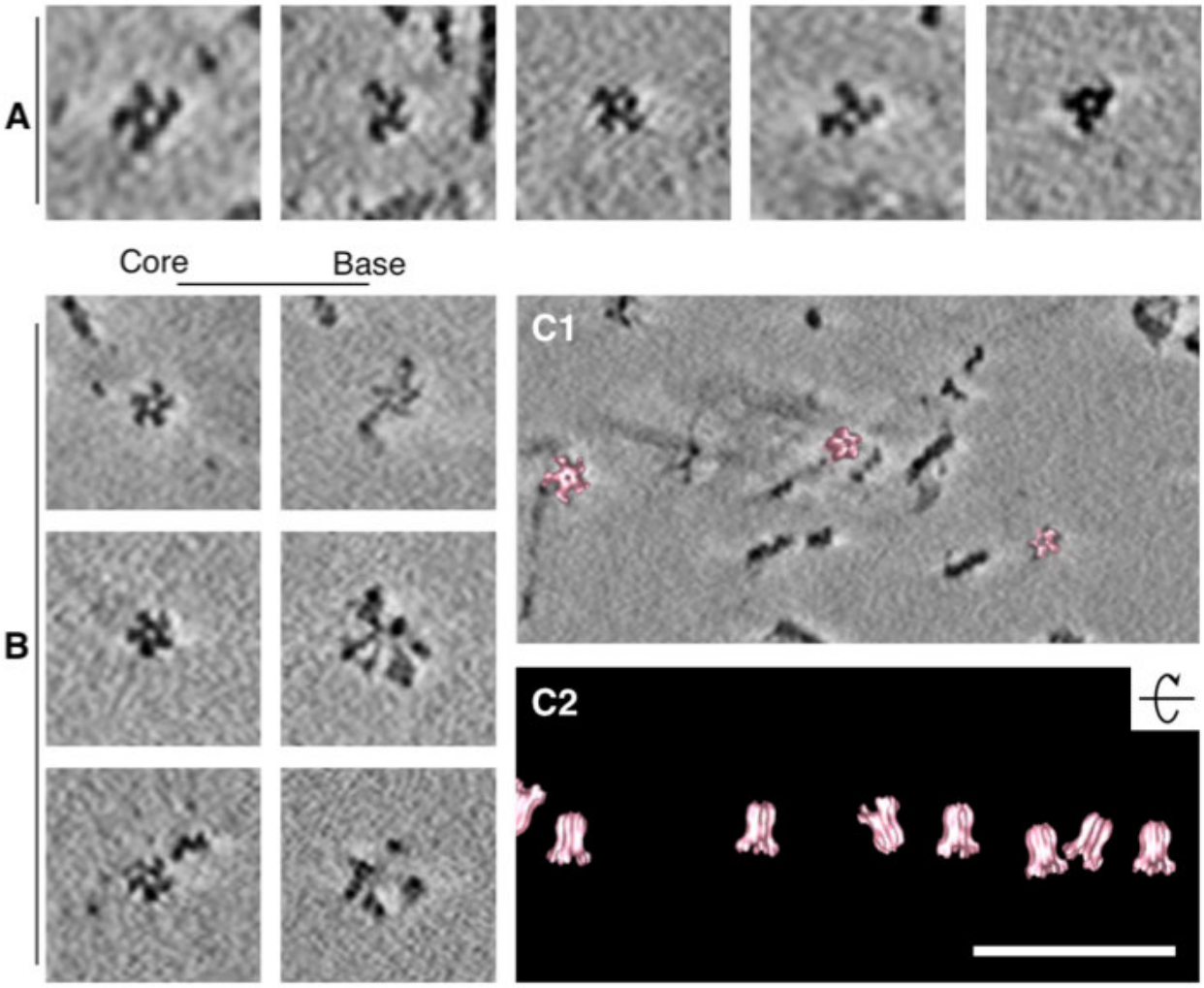
A
Core
Base
B
C1
C2


D

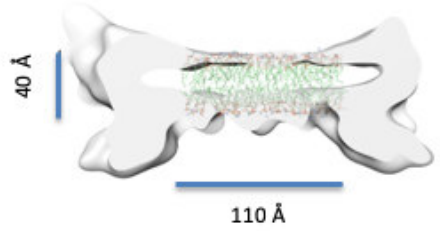
E
40 Å
110 Å

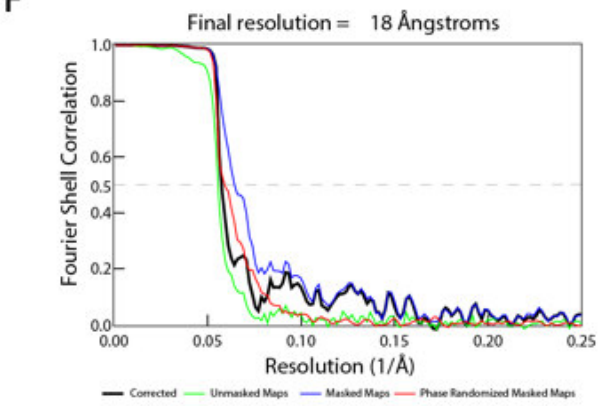
F
Final resolution = 18 Ångstroms
Fourier Shell Correlation
1.0
0.8
0.6
0.5
0.4
0.2
0.0
0.00
0.05
0.10
0.15
0.20
0.25
Resolution (1/Å)
Corrected
Unmasked Maps
Masked Maps
Phase Randomized Masked Maps

Appendix Figure S4

In situ and in vitro characterization of the core and base

A Cryotomographic slices through top views of purified TssJLM particles. Particles were often incomplete and seemed to possess only 3 or 4 of the 5 branches that were usually seen in cells. Scale bar 10 nm.

B Shown are two slices at different heights of 3 different complete (5-branched stars) TssJLM particles, highlighting the flexibility of the base. The first column shows the stable star shape found at the core (height A in Fig. 1), and the second column shows the flexible densities found at the base (height E in Fig 1). Scale bar 10 nm.

C1, C2 Slice through a tomogram of purified TssJLM particles. The average shown in Figure 1 was placed back into this tomogram. The view in (C1) is parallel to the beam axis, while the view in (C2) is flipped 90° and parallel to the ice surface and only the isosurfaces are shown. The ice is very thin (~30 nm). Scale bar 100 nm

D. 2D classes of the subtracted base of the ME complex

E. Cross section of the cryo-EM reconstruction of the subtracted base with the PE lipid leaflets as an atom representation for comparison.

F FSC curve of the subtracted base cryo-EM density. The cut-off used was 0.5 to determine the resolution.

Appendix Figure S5

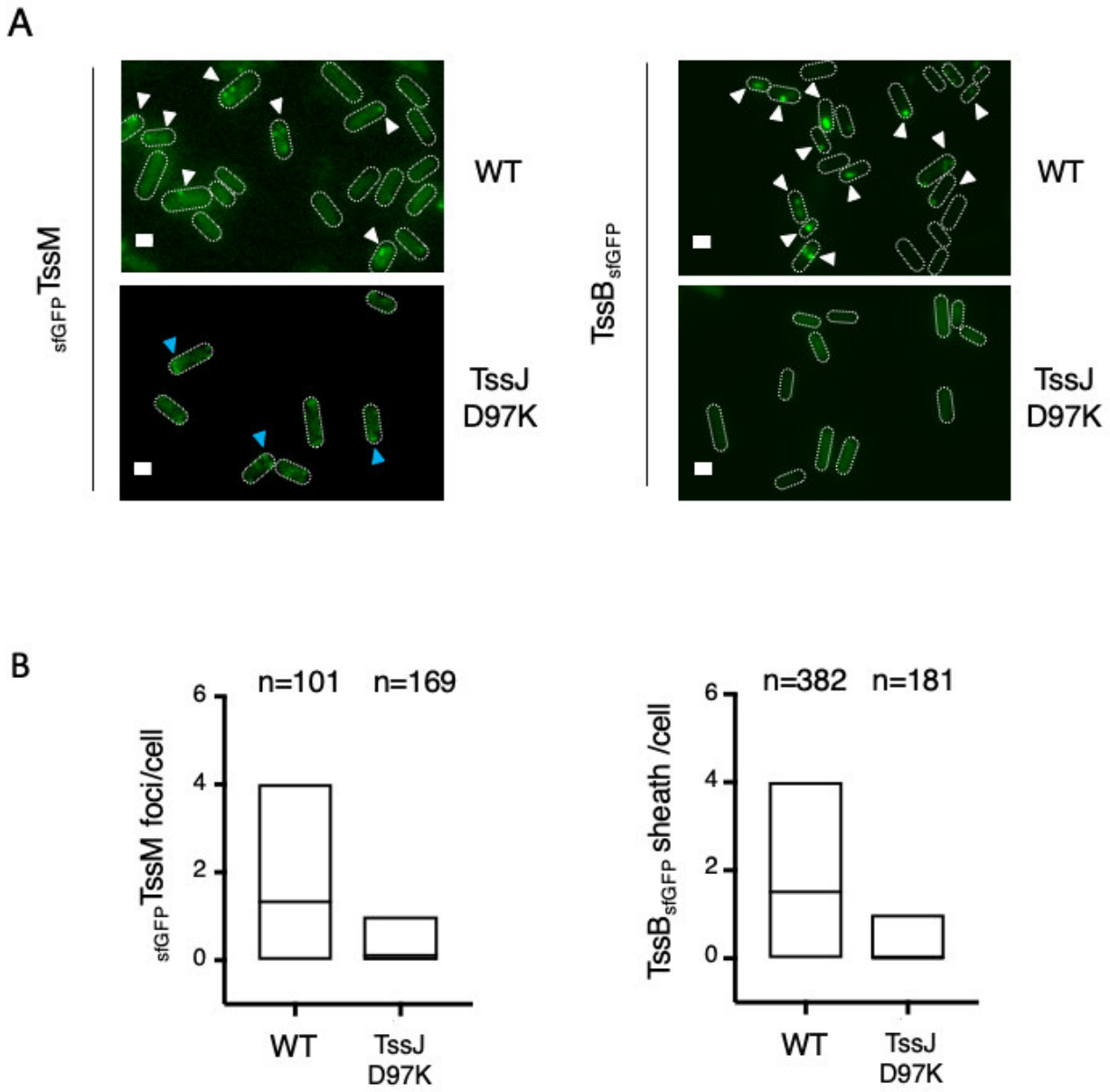

Appendix Figure S5

Disruption of TssJ' recruitment impacts membrane complex stability.

A (Left) Fluorescence microscopy recordings showing sfGFPTssM foci in the parental (WT) and TssJ mutated strains (TssJ D97K). TssM foci containing cells are indicated by arrowheads. (Right) Fluorescence microscopy recordings showing TssBsfGFP sheath in the parental (WT) and TssJ mutated strains (TssJ D97K). Fluorescent sheath containing cells are indicated by arrowheads. Microscopy analyses were performed independently three times, each in technical triplicate, and a representative experiment is shown. Scale bars, 1 µm

B TssJ' recruitment is essential for in vivo membrane complex assembly. Statistical analysis of $_{sfGFP}$TssM foci and TssB$_{sfGFP}$ sheath in various T6SS background. Shown are floating bars of the measured number of $_{sfGFPT}$ssM foci (left) and TssB$_{sfGFP}$ sheath (right) per cell in the parental (WT) and TssJ mutated strains (TssJ D97K). Lower and upper boundaries of the boxes correspond respectively to the minimum and maximum value, the mean is represented by a black line. The number of cells analysed for each strain is indicated on top

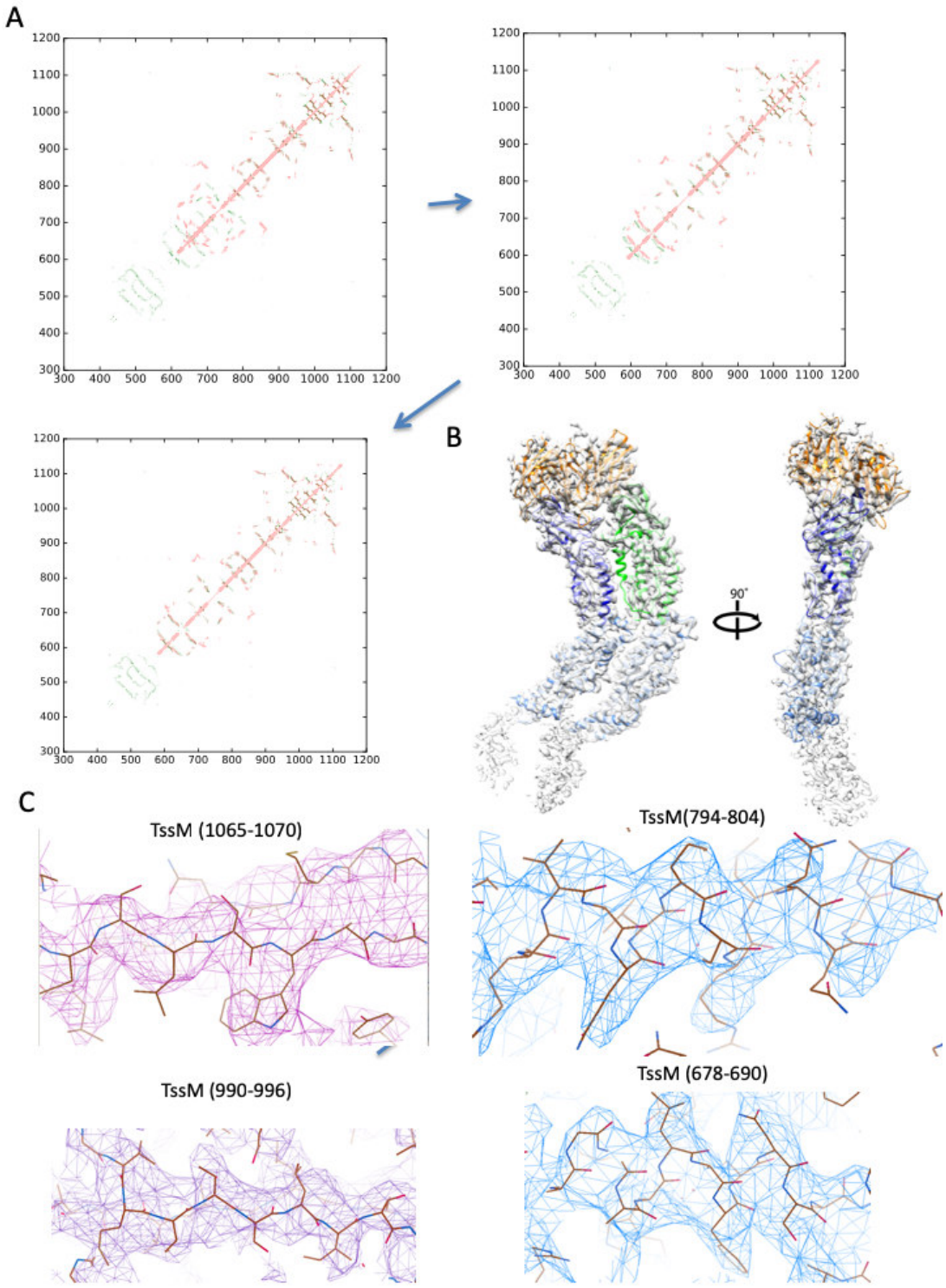

Appendix Figure S6

TssM model building and validation

A Comparison of the predicted contacts (in green) and the contact map of the built pseudoatomc model (in red).

B Fitting of the known structure in orange, blue and green and the *de novo* built pseudoatomic model in light blue. Two orientations are shown. The locally sharpened cryo-EM density is transparent

C Representative pseudoatomic model fitting in the cryo-EM density, either of the crystal structure (in pink) and built *de novo* (in light blue)

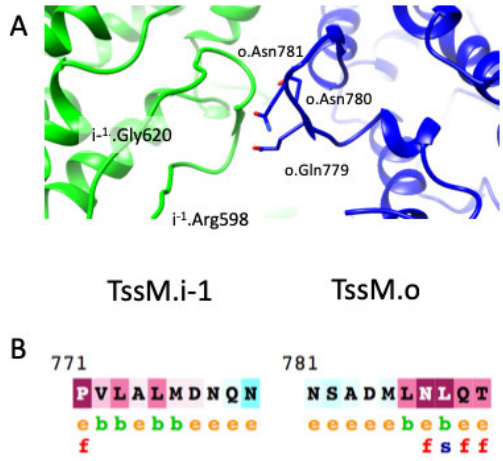

Appendix Figure S7

The periplasmic gate

A The periplasmic gate loop in the external pillar interacts with a loop of the inner pillar. In blue is the external pillar TssM.o and in green is the internal pillar TssM.i^{-1}. The amino acids involved in the interaction are shown in atom form

B The periplasmic gate sequence is not conserved. In Cyan is the less conserved sequence and in magenta is the most conserved

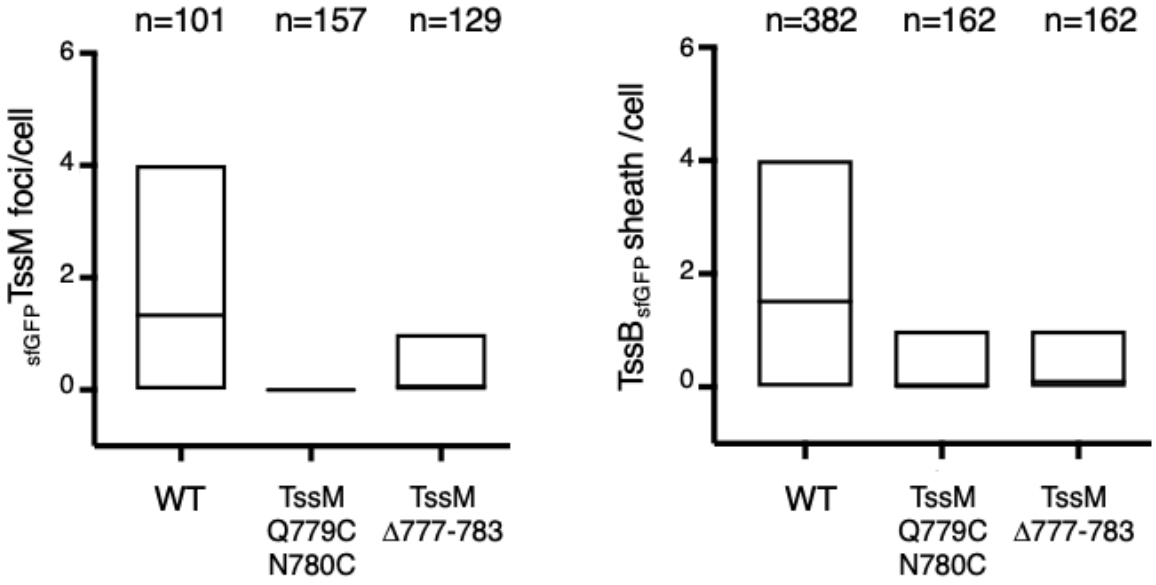

Appendix Figure S8

TssM channel integrity is necessary for in vivo membrane complex biogenesis.

Statistical analysis of sfGFPTssM foci and TssBsfGFP sheath in various T6SS background. Shown are floating bars of the mesured number of sfGFPTssM foci (left) and TssBsfGFP sheath (right) per cell in the parental (WT) and TssM mutated strains (TssM Q779C/N780C, TssM Δ777-783). Lower and upper boundaries of the boxes correspond respectively to the minimum and maximum value, the mean is represented by a black line. The number of cells analyzed for each strain is indicated on top

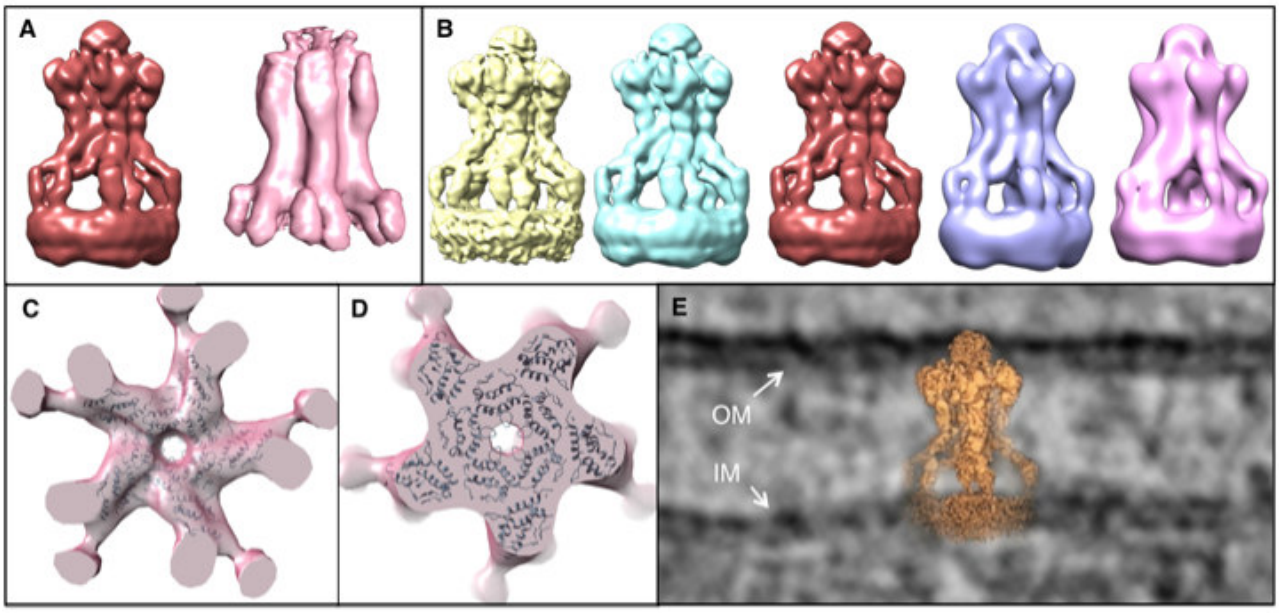

Appendix Figure S9

Cryo-EM and cryo-ET structure comparison.

A Comparison of the SPA full structure (presented in Fig 3) low pass filtered at 20 Å (left, carmine) with the final cryo-ET average (right, light pink)

B Comparison of the SPA full structure (presented in Fig 3) low pass filtered at 10, 15, 20, 25 and 30 Å form left to right

C, D Pseudo-atomic model derived from the SPA structure (see Fig 5A) docked into the *in situ* subtomogram average. Isosurface and atomic models were clipped to highlight the position of the loop within the central channel. (C) represents a bottom view clipped around height D in Fig 1. (D) represents a top view clipped around height E in Fig 1

E Cryo-EM SPA structure replaced manually in the tomogram of a FIB-milled BL21 cell

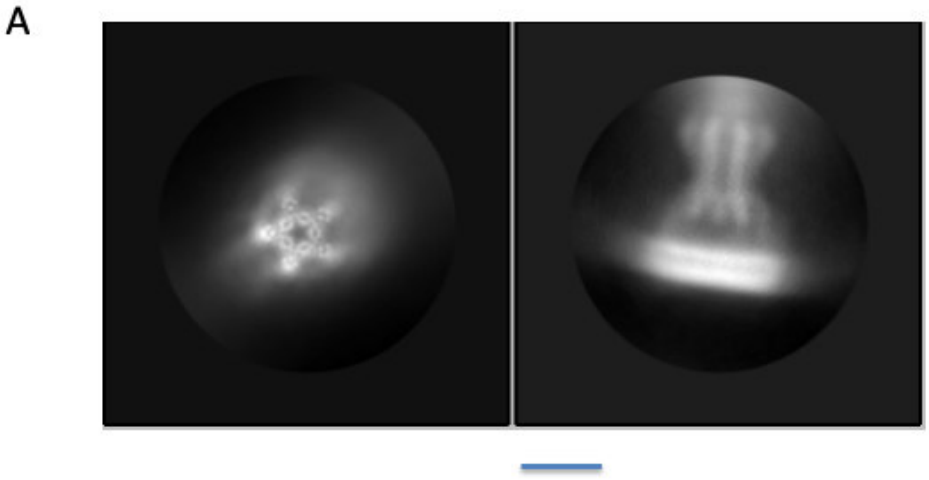

Appendix Figure S10

The membrane complex in amphipols

A 2D class averages of the MC in amphipols. The scale bar represents 100 Å

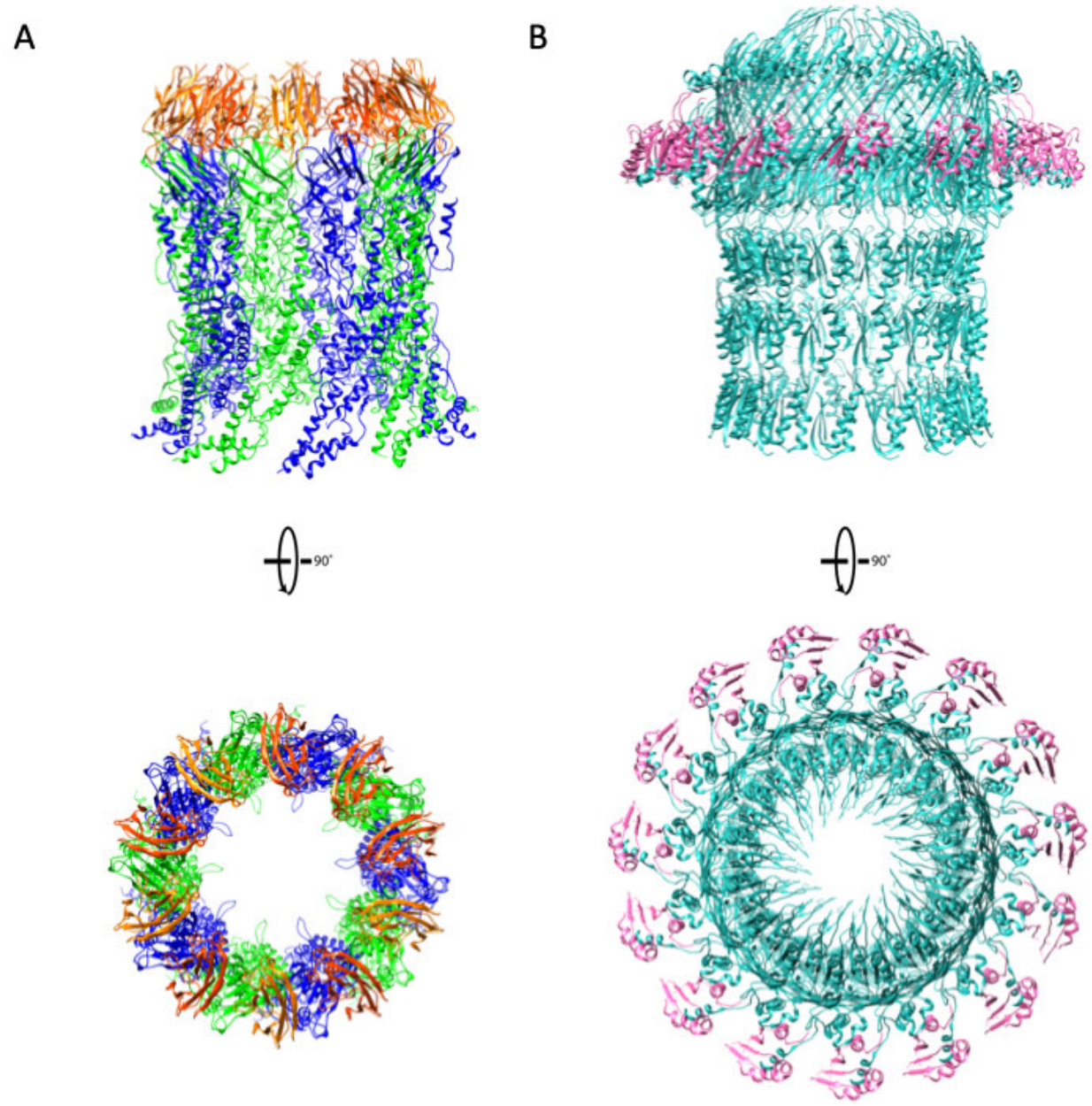

Appendix Figure S11

Open conformation model

A The pseudoatomic model of an open conformation of the MC, based on molecular dynamics simulation previously published (Durand *et al*, 2015). In green and in blue are the internal and external pillars, respectively and the TssJ protomers are in orange. Two views are shown

B The pseudoatomic model of GspD (in light sea green), from E.coli (**5zdh**) with its pilotin (in hot pink)(Yin *et al*, 2018). Two views are shown

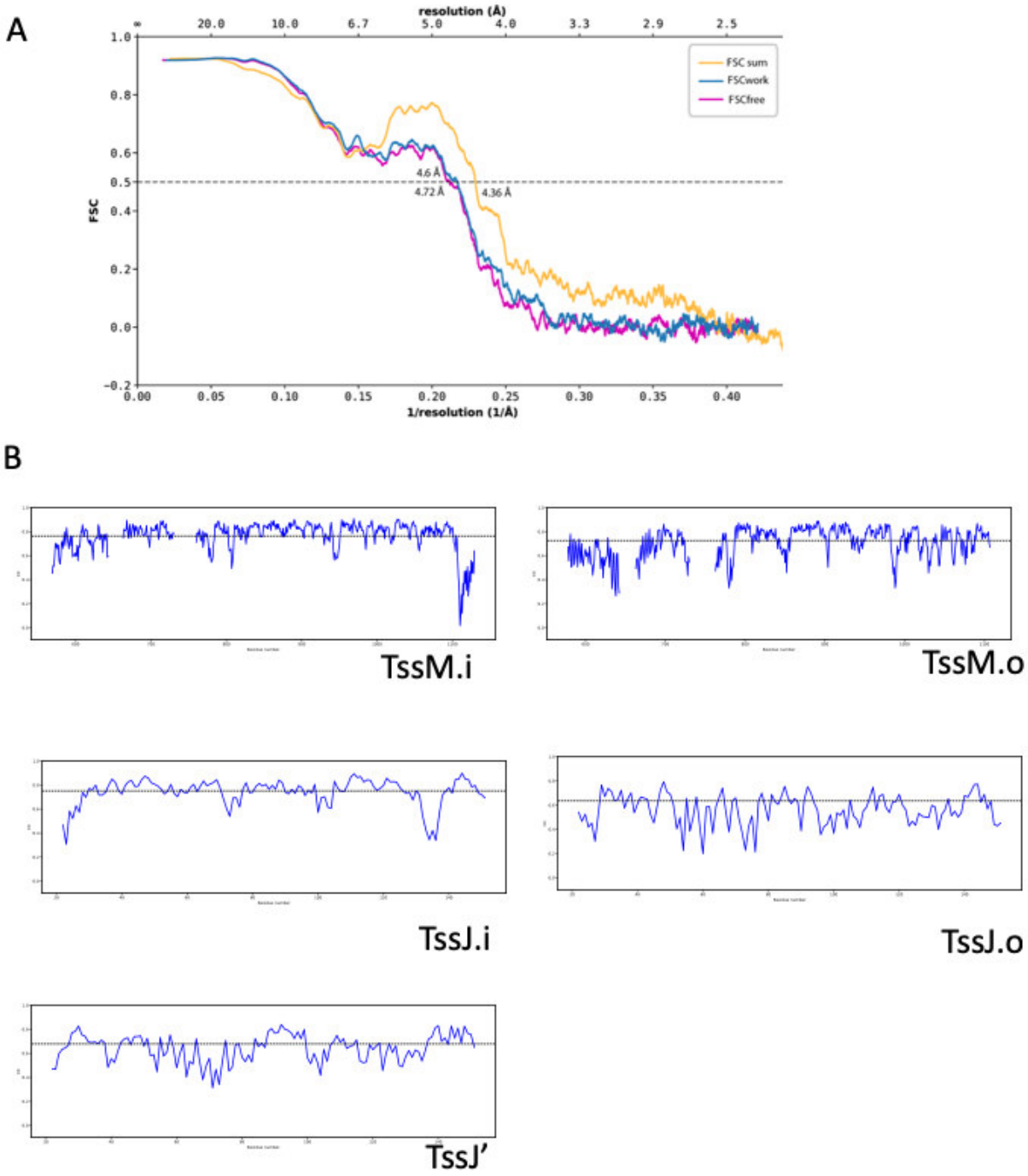

Appendix Figure S12

Validation of the pseudoatomic model

A The model to map FSC curve of the sharpened map vs model (FSCsum, orange), the shaken (0.5Å) model vs one Half map (FSCwork, blue) and the latter model against the other Half map (FSCfree, magenta)

B Cross-correlation graphs of each amino acid to the sharpened cryo-EM map, for each chain

Tables

Appendix Table S1

Reagents and resources

REAGENT or RESOURCE	SOURCE	
Bacterial Strains		
DH5α	New England Biolabs	Cat# C2987I
W3110	Laboratory collection	N/A
BL21 (DE3)	New England Biolabs	Cat# C2527I
BL21(DE3) Δ*minCDE*Ω*kan*	This study	N/A
BL21(DE3) *mreB*^{A125V}	This study	N/A
BL21(DE3) *mreB*^{A125V} Δ*minCDE*Ω*kan*	This study	N/A
BL21(DE3) *mreB*^{A125V} Δ*minCDE*Ω*cm*	This study	N/A
Enteroaggregative *E. coli* strain 17-2	Laboratory collection	N/A
Enteroaggregative *E. coli* strain 17-2 *tssJ* (R31E)	This study	N/A
Enteroaggregative *E. coli* strain 17-2 *tssJ* (D97A)	This study	N/A
Enteroaggregative *E. coli* strain 17-2 *tssJ* (D97K)	This study	N/A
Enteroaggregative *E. coli* strain 17-2 *tssM* (Q779C)	This study	N/A
Enteroaggregative *E. coli* strain 17-2 *tssM* (Q779C/N780C)	This study	N/A
Enteroaggregative *E. coli* strain 17-2 *tssM* (Δ777-783K)	This study	N/A
Enteroaggregative *E. coli* strain 17-2-$_{sfGFP}$*tssM*	(Durand *et al*, 2015)	N/A
Enteroaggregative *E. coli* strain 17-2 *tssJ* (R31E)-$_{sfGFP}$*tssM*	This study	N/A
Enteroaggregative *E. coli* strain 17-2 *tssJ* (D97A)-$_{sfGFP}$*tssM*	This study	N/A
Enteroaggregative *E. coli* strain 17-2 *tssJ* (D97K)-$_{sfGFP}$*tssM*	This study	N/A
Enteroaggregative *E. coli* strain 17-2 *tssM* (Q779C)-$_{sfGFP}$*tssM*	This study	N/A
Enteroaggregative *E. coli* strain 17-2 *tssM* (Q779C/N780C)-$_{sfGFP}$*tssM*	This study	N/A
Enteroaggregative *E. coli* strain 17-2 *tssM* (Δ777-783K) $_{sfGFP}$*tssM*	This study	N/A
Enteroaggregative *E. coli* strain 17-2-*tssB*$_{sfGFP}$	(Brunet *et al*, 2013)	N/A
Enteroaggregative *E. coli* strain 17-2 *tssJ* (R31E) -*tssB*$_{sfGFP}$	This study	N/A
Enteroaggregative *E. coli* strain 17-2 *tssJ* (D97A) -*tssB*$_{sfGFP}$	This study	N/A
Enteroaggregative *E. coli* strain 17-2 *tssJ* (D97K) -*tssB*$_{sfGFP}$	This study	N/A
Enteroaggregative *E. coli* strain 17-2 *tssM* (Q779C) -*tssB*$_{sfGFP}$	This study	N/A
Enteroaggregative *E. coli* strain 17-2 *tssM* (Q779C/N780C) -*tssB*$_{sfGFP}$	This study	N/As
Enteroaggregative *E. coli* strain 17-2 *tssM* (Δ777-783K) -*tssB*$_{sfGFP}$	This study	N/A
Enteroaggregative *E. coli* strain 17-2 *mreB*^{A125V}	This study	N/A
Chemicals, Peptides, and Recombinant Proteins		
HisTrap high performance (5mL)	GE Healthcare	Cat# GE17-5248-01
StrepTrap high performance (5mL)	GE Healthcare	Cat# GE28-9075-47
Superose 6 increase 10/300 GL	GE Healthcare	Cat# GE29-0915-96
cOmplete™ ULTRA Tablets, EDTA-free, glass vials Protease Inhibitor Cocktail	Roche	Cat# 05892953001
DNase I	Roche	Cat# 10104159001
Lysozyme	Sigma-Aldrich	Cat# 62971
Imidazole	Sigma-Aldrich	Cat# 56750

Hepes	Sigma-Aldrich	Cat# H3375
Acrylamide/Bis-Acrylamide 37.5:1, 40%	Biosolve	Cat# 001422335BS
Graphene Oxide solution	Sigma	Cat# 763705

Recombinant DNA		
pKD4	(Datsenko & Wanner, 2000)	Addgene #45605
pKOBEG	(Chaveroche *et al*, 2000)	N/A
pCP20	(Cherepanov & Wackernagel, 1995)	N/A
pKO3	(Link *et al*, 1997)	N/A
pKO3-TssJ	This study	N/A
pKO3-TssM	This study	N/A
pRSF-Duet1	Novagen	#71341-3
pRSF-TssJ^{H}-^{Flag}L-^{His}M	(Durand *et al*, 2015)	N/A
pBAD33- TssJ^{H}-^{Flag}L-^{His}M	This study	N/A

Software and Algorithms		
Coot	(Emsley *et al*, 2010)	https://www2.mrc-lmb.cam.ac.uk/personal/pemsley/coot/
Coot trimmings	(Clarke, 2017)	https://github.com/olibclarke/coot-trimmings
Cryosparc 0.6	(Punjani *et al*, 2017)	https://cryosparc.com/
Csparc2star.py	(Asarnow, 2016)	https://github.com/asarnow/pyem/blob/master/csparc2star.py
EMRinger	(Barad *et al*, 2015)	http://emringer.com/
gCTF	(Zhang, 2016)	https://www.mrc-lmb.cam.ac.uk/kzhang/Gctf/
i-TASSER	(Wang *et al*, 2017)	https://zhanglab.ccmb.med.umich.edu/I-TASSER/
ImageJ	(Schneider *et al*, 2012)	https://imagej.net/ImageJ
IMOD	(Kremer *et al*, 2005)	https://bio3d.colorado.edu/imod/
MapAlign	(Ovchinnikov *et al*, 2017)	https://github.com/sokrypton/map_align
MicrobeJ	(Ducret *et al*, 2016)	http://www.microbej.com/index.html
MolProbity	(Chen *et al*, 2010)	http://molprobity.biochem.duke.edu/
MotionCor2	(Zheng *et al*, 2017)	http://msg.ucsf.edu/em/software/motioncor2.html
PEET	(Nicastro et al, 2006)	https://bio3d.colorado.edu/PEET
Phenix	(Adams *et al*, 2010)	https://www.phenix-online.org/
Phenix real-space refine	(Afonine *et al*, 2018)	https://www.phenix-online.org/
Phyre2	(Kelley *et al*, 2015)	http://www.sbg.bio.ic.ac.uk/phyre2/html/page.cgi?id=index
PISA	(Krissinel & Henrick, 2007)	http://www.ebi.ac.uk/pdbe/pisa/
RaptorX	(Wang *et al*, 2017)	http://raptorx.uchicago.edu/ContactMap/
RELION 2.1	(Scheres, 2012)	http://www2.mrc-lmb.cam.ac.uk/relion/index.php/Download_%26_install
Rosetta	(Leaver-Fay *et al*, 2011)	https://www.rosettacommons.org/software
SerialEM	(Mastronarde, 2005)	http://bio3d.colorado.edu/SerialEM/
UCSF Chimera	(Pettersen *et al*, 2004)	https://www.cgl.ucsf.edu/chimera
UCSF Tomo	(Zheng *et al,* 2007)	http://www.msg.ucsf.edu/Tomography

Protein accession numbers		
TssJ	WP_000974469.1	type VI secretion system lipoprotein TssJ [Escherichia]
TssL	WP_001040045.1	DotU family type IV/VI secretion system protein [Escherichia coli]
TssM	KDW08523.1	type VI secretion protein IcmF [Escherichia coli 2-156-04_S3_C3]

Other		
Talos Arctica	Thermo scientific	https://www.fei.com/products/tem/talos-arctica-for-life-sciences/
Falcon 3EC	Thermo scientific	https://www.fei.com/accessories/falcon-3ec-direct-electron-detector/
Leica EM GP	Leica	https://www.leica-microsystems.com/products/sample-preparation-for-electron-microscopy/cryo-preparation-systems/details/product/leica-em-gp-1/
ÄKTA Avant	GE Healthcare Life Sciences	https://www.gelifesciences.com/en/us/shop/chromatography/chromatography-systems/akta-avant-p-06264

Deposited Data		
EAEC TssJLM core complex	This paper, deposited at EMdatabank	EMD-0264
EAEC TssJLM ccomplex	This paper, deposited at EMdatabank	EMD-0265
EAEC TssJLM ccomplex (C1)	This paper, deposited at EMdatabank	EMD-0266
EAEC TssJLM base complex	This paper, deposited at EMdatabank	EMD-0267
EAEC TssJLM complex	This paper, deposited at PDB	PDB 6HS7

Appendix Table S2

Oligonucleotides

Name	Destination	Sequence (5'➔3')
For plasmid construction [a,b]		
pKO3-*tssJ*		FWD: ATT**GCGGCCGC**GCATCATGACCGACGACGGATCC REV: ATT**GCGGCCGC**GCACGTAGCGCTGCTGTTTCAG
pKO3-*tssM*		FWD: ATT**GGATCC**GAACAGCGATGCCATGCTGTATCAG REV: ATT**GTCGAC**GCGCAGCTCAAAATGCAGCCCCG
pKO3-*tssJ* (R31E)	Mutagenesis of the pKO3-*tssJ*	FWD:AAACACTTCACCTGGATATT*GAA*GCCAGGGAGGCCATTAACAC REV:GTGTTAATGGCCTCCCTGGC*TTC*AATATCCAGGTGAAGTGTTT
pKO3-*tssJ* (D97A)	Mutagenesis of the pKO3-*tssJ*	FWD :CCAGGTGGTTCAGTAGCCGTGG*C*TATGCCTCTGGATGATGCGGC REV:GCCGCATCATCCAGAGGCATA*G*CCACGGCTACTGAACCACCTGG
pKO3-*tssJ* (D97K)	Mutagenesis of the pKO3-*tssJ*	FWD: GGTGGTTCAGTAGCCGTG*AAA*ATGCCTCTGGATGATGCGG REV: CCGCATCATCCAGAGGCAT*TTT*CACGGCTACTGAACCACC
pKO3-*tssM* (Q779C)	Mutagenesis of the pKO3-*tssM*	FWD: TGCTTGCACTGATGGATAAT*TGT*AACAACAGTGCGGATATGCT REV: AGCATATCCGCACTGTTGTT*ACA*ATTATCCATCAGTGCAAGC
pKO3-*tssM* (Q779C/N780C)	Mutagenesis of the pKO3-*tssM*	FWD: TGCTTGCACTGATGGATAAT*TGTTG*CAACAGTGCGGATATGCT REV: AGCATATCCGCACTGTTG*CAACA*ATTATCCATCAGTGCAAGCA
pKO3-*tssM* (Δ777-783)	Mutagenesis of the pKO3-*tssM*	FWD: CGGTGCTTGCACTGATGATGCTGAATCTGCAGACATA REV: TATGTCTGCAGATTCAGCATCATCAGTGCAAGCACCG
For strain construction [c]		
17-2-*tssJ*(R31E)-$_{sfGFP}$*tssM**	Chromosomic fusion of the *sfGFP* gene to the N-term region of *tssM*	FWD:TTCTCATCCGGAGAAGAACATTTTATCAGTACTGTTACATCAGGAAA CCAGAATGAATAACGATTGTGTAGGCTGGAGCTGCTTCGAAGTTCCTATA C REV:CACACCAATAAATACAATCCCCGGTCGCCCAAAGCGACCAGACAGA CAGGCCAGTTTATTCCCTCCGCCGGCCGCTGC
17-2-*tssJ*(R31E)-*tssB*$_{sfGFP}$**	Chromosomic fusion of the *sfGFP* gene to the C-term region of *tssB*	FWD:CCGGCACTGAGTCAGACGCTGCGTGATGAACTGCGTGCACTGGTG CCGGAAAAGGCGGCAGCGGCCGGCGGAGGG REV:GCAACGTTCTTTTCTTTCTGTACAGACATCAGCATTTTCTCTCGTAA TCCGTTAAACATATGAATATCCTCCTTAGTTCCTATTCCGAAGTTCC
Del-minCDE-DW	Deletion of the minCDE operon in BL21	FWD:AACATCATCGCGCGCTGGCGATGATTAATAGCTAATTGAGTAAGGC CAGGTGTGTAGGCTGGAGCTGCTTC REV:CAAGGCAGAGATAACTCTGCCTTGAAGATAAATGCGCTTTTACAGCG GGCCATATGAATATCCTCCTTAGTTC

*same oligonucleotides used to chromosomally fuse the *sfGFP* gene in the N-term region of *tssM* in the 17-2-*tssJ* (D97A), 17-2-*tssJ* (D97K), 17-2-*tssM* (Q779C), 17-2-*tssM* (Q779C/N780C) and 17-2-*tssM* (*Δ777-783) strains.*

**same oligonucleotides used to chromosomally fuse the *sfGFP* gene in the C-term region of *tssB* in the 17-2-*tssJ* (D97A), 17-2-*tssJ* (D97K), 17-2-*tssM* (Q779C), 17-2-*tssM* (Q779C/N780C) and 17-2-*tssM* (*Δ777-783) strains.*

[a] residue mutated *italicized*

[b] restriction site in **bold**

[c] sequence annealing to the target vector underlined

Appendix References

Adams PD, Afonine P V., Bunkóczi G, Chen VB, Davis IW, Echols N, Headd JJ, Hung L-W, Kapral GJ, Grosse-Kunstleve RW, McCoy AJ, Moriarty NW, Oeffner R, Read RJ, Richardson DC, Richardson JS, Terwilliger TC & Zwart PH (2010) PHENIX: a comprehensive Python-based system for macromolecular structure solution. *Acta Crystallogr. D. Biol. Crystallogr.* **66:** 213–21

Afonine P V., Poon BK, Read RJ, Sobolev O V., Terwilliger TC, Urzhumtsev A & Adams PD (2018) Real-space refinement in PHENIX for cryo-EM and crystallography. *Acta Crystallogr. Sect. D Struct. Biol.* **74:** 531–544

Asarnow D (2016) Pyem. *GitHub* Available at: https://github.com/asarnow/pyem

Barad BA, Echols N, Wang RY-R, Cheng Y, DiMaio F, Adams PD & Fraser JS (2015) EMRinger: side chain–directed model and map validation for 3D cryo-electron microscopy. *Nat. Methods* **12:** 943–946

Brunet YR, Espinosa L, Harchouni S, Mignot T & Cascales E (2013) Imaging Type VI Secretion-Mediated Bacterial Killing. *Cell Rep.* **3:** 36–41

Chaveroche MK, Ghigo JM & d'Enfert C (2000) A rapid method for efficient gene replacement in the filamentous fungus Aspergillus nidulans. *Nucleic Acids Res.* **28:** E97

Chen VB, Arendall WB, Headd JJ, Keedy DA, Immormino RM, Kapral GJ, Murray LW, Richardson JS & Richardson DC (2010) MolProbity : all-atom structure validation for macromolecular crystallography. *Acta Crystallogr. Sect. D Biol. Crystallogr.* **66:** 12–21

Cherepanov PP & Wackernagel W (1995) Gene disruption in Escherichia coli: TcR and KmR cassettes with the option of Flp-catalyzed excision of the antibiotic-resistance determinant. *Gene* **158:** 9–14

Clarke OB (2017) Coot Trimmings.

Datsenko KA & Wanner BL (2000) One-step inactivation of chromosomal genes in Escherichia coli K-12 using PCR products. *Proc. Natl. Acad. Sci.* **97:** 6640–6645

Ducret A, Quardokus EM & Brun Y V. (2016) MicrobeJ, a tool for high throughput bacterial cell detection and quantitative analysis. *Nat. Microbiol.* **1:** 16077

Durand E, Nguyen VS, Zoued A, Logger L, Péhau-Arnaudet G, Aschtgen M-S, Spinelli S, Desmyter A, Bardiaux B, Dujeancourt A, Roussel A, Cambillau C, Cascales E & Fronzes R (2015) Biogenesis and structure of a type VI secretion membrane core complex. *Nature* **523:** 555–560

Emsley P, Lohkamp B, Scott WG & Cowtan K (2010) Features and development of Coot. *Acta Crystallogr. Sect. D Biol. Crystallogr.* **66:** 486–501

Kelley LA, Mezulis S, Yates CM, Wass MN & Sternberg MJE (2015) The Phyre2 web portal for protein modeling, prediction and analysis. *Nat. Protoc.* **10:** 845–858

Krissinel E & Henrick K (2007) Inference of Macromolecular Assemblies from Crystalline State. *J. Mol. Biol.* **372:** 774–797

Leaver-Fay A, Tyka M, Lewis SM, Lange OF, Thompson J, Jacak R, Kaufman K, Renfrew PD, Smith CA, Sheffler W, Davis IW, Cooper S, Treuille A, Mandell DJ, Richter F, Ban YEA, Fleishman SJ, Corn JE, Kim DE, Lyskov S, et al (2011) Rosetta3: An object-oriented software suite for the simulation and design of macromolecules. *Methods Enzymol.* **487:** 545–574

Link AJ, Phillips D & Church GM (1997) Methods for generating precise deletions and insertions in the genome of wild-type Escherichia coli: application to open reading frame characterization. *J. Bacteriol.* **179:** 6228–6237

Ovchinnikov S, Park H, Varghese N, Huang P-S, Pavlopoulos GA, Kim DE, Kamisetty H, Kyrpides NC & Baker D (2017) Protein structure determination using metagenome sequence data. *Science (80-.).* **355:** 294–298

Pettersen EF, Goddard TD, Huang CC, Couch GS, Greenblatt DM, Meng EC & Ferrin TE (2004) UCSF Chimera--a visualization system for exploratory research and analysis. *J. Comput. Chem.* **25:** 1605–12

Punjani A, Rubinstein JL, Fleet DJ & Brubaker MA (2017) cryoSPARC: algorithms for rapid unsupervised cryo-EM structure determination. *Nat. Methods* **14:** 290–296

Scheres SHWW (2012) RELION: implementation of a Bayesian approach to cryo-EM structure determination. *J. Struct. Biol.* **180:** 519–30

Schneider CA, Rasband WS & Eliceiri KW (2012) NIH Image to ImageJ: 25 years of image analysis. *Nat. Methods* **9:** 671–5

Wang S, Sun S, Li Z, Zhang R & Xu J (2017) Accurate De Novo Prediction of Protein Contact Map by Ultra-Deep Learning Model. *PLOS Comput. Biol.* **13:** e1005324

Yin M, Yan Z & Li X (2018) Structural insight into the assembly of the type II secretion system pilotin-secretin complex from enterotoxigenic Escherichia coli. *Nat. Microbiol.* **3:** 581–587

Zhang K (2016) Gctf: Real-time CTF determination and correction. *J. Struct. Biol.* **193:** 1–12

Zheng SQ, Palovcak E, Armache J-P, Verba KA, Cheng Y & Agard DA (2017) MotionCor2: anisotropic correction of beam-induced motion for improved cryo-electron microscopy. *Nat. Methods* **14:** 331–332